

Article

The Resource Utilization of Poplar Leaves for CO₂ Adsorption

Xia Wang ^{1,*} , Fanyuan Kong ², Wulan Zeng ¹, Huaxiang Zhang ¹, Chunling Xin ¹ and Xiangjun Kong ¹¹ Department of Chemistry and Chemical Engineering, Weifang University, Weifang 261061, China² Library, Weifang University, Weifang 261061, China

* Correspondence: 20160012@wfu.edu.cn

Abstract: Every late autumn, fluttering poplar leaves scatter throughout the campus and city streets. In this work, poplar leaves were used as the raw material, while H₃PO₄ and KOH were used as activators and urea was used as the nitrogen source to prepare biomass based-activated carbons (ACs) to capture CO₂. The pore structures, functional groups and morphology, and desorption performance of the prepared ACs were characterized; the CO₂ adsorption, regeneration, and kinetics were also evaluated. The results showed that H₃PO₄ and urea obviously promoted the development of pore structures and pyrrole nitrogen (N-5), while KOH and urea were more conducive to the formation of hydroxyl (–OH) and ether (C–O) functional groups. At optimal operating conditions, the CO₂ adsorption capacity of H₃PO₄- and KOH-activated poplar leaves after urea treatment reached 4.07 and 3.85 mmol/g, respectively, at room temperature; both showed stable regenerative behaviour after ten adsorption–desorption cycles.

Keywords: activated carbons; activation; nitrogen doping; CO₂ adsorption; regeneration



Citation: Wang, X.; Kong, F.; Zeng, W.; Zhang, H.; Xin, C.; Kong, X. The Resource Utilization of Poplar Leaves for CO₂ Adsorption. *Molecules* **2024**, *29*, 2024. <https://doi.org/10.3390/molecules29092024>

Academic Editor: Juan Antonio Cecilia

Received: 13 March 2024

Revised: 18 April 2024

Accepted: 25 April 2024

Published: 27 April 2024



Copyright: © 2024 by the authors. Licensee MDPI, Basel, Switzerland. This article is an open access article distributed under the terms and conditions of the Creative Commons Attribution (CC BY) license (<https://creativecommons.org/licenses/by/4.0/>).

1. Introduction

Currently, excessive CO₂ emissions cause serious greenhouse gas (GHG) effects and increase the burden of achieving dual carbon targets. Liquid absorption and solid adsorption methods have been widely studied for separating CO₂ from large CO₂ emission points [1–4]. To date, liquid absorption technology has been applied in industry, but the most commonly used liquid amines have the disadvantages of easy degradation, high regeneration energy consumption, and strong corrosion at equilibrium [5–9]. The solid adsorption method is well approved due to its good adsorption capacity, low corrosiveness, and low degradation [10,11]. Solid sorbents, such as molecular sieves [9,12,13], metal-organic frameworks (MOFs) [14–17], carbon nanotubes [18], microporous carbons [19–23], and other synthetic and modified materials [24–34], exhibit good CO₂ adsorption performance. However, the synthesis costs of these sorbents are usually high, which undoubtedly hinders their wide application.

Realizing effective CO₂ capture at large CO₂ emission points at low costs is a significant contribution. In late autumn in China, large amounts of waste biomass, such as agricultural waste and leaves, are stacked in disorderly fashion and burned traditionally, causing serious environmental pollution problems and hindering dual carbon targets. The resource utilization of biomass waste is undoubtedly a win-win situation.

Many researchers have conducted extensive studies on realizing the resource utilization of biomass as a carrier of catalyst or an adsorbent for gas and heavy metals [35–54]. Zhang et al. designed poly(acrylic acid)-grafted chitosan and rice straw-based biochar to adsorb heavy metals in wastewater, which suggested selective adsorption of Cr³⁺, Pb²⁺, and Cu²⁺ [36]. Ding et al. prepared seaweed-based porous biochars from *Sargassum* and *Enteromorpha* using a KOH activation method, and CO₂ adsorption capacities of 1.05 and 0.52 mmol/g were reached for both at room temperature [37]. Xu et al. prepared N-doped biochars from waste walnut shells by using urea as the nitrogen source, H₃PO₄ as the pretreatment agent and KOH, K₂CO₃, and ZnCl₂ as activators; the results

showed that different activators suggested different effects on improving the pore structure and N content. The CO₂ adsorption capacity of ZnCl₂-activated waste walnut shells was 0.6 mmol/g at 25 °C and 0.15 bar [41]. Ello et al. prepared microporous biocarbon materials from African palm shells using a KOH-activation method; the specific surface area ranged from 365 to 1890 m²/g, the pore volume ranged from 0.16 to 0.82 cm³/g, and the CO₂ adsorption capacity was 4.4 mmol/g at 25 °C and 1 bar [43]. Plaza et al. produced microporous biochars from almond shells using one-step activation with an O₂ concentration of 3–5% in a N₂ atmosphere at 500–650 °C, and the results showed that the developed narrow microporosity promoted CO₂ adsorption at low partial pressures [47]. Our research group also prepared corncob- and peanut-shell-based activated carbons using an alkali activation method, which exhibited developed pore structures and good CO₂ adsorption performance [50,51].

Poplars are among the most common green tree species in China, and poplar leaves also scatter on roads in late autumn; therefore, understanding the resource utilization of poplar leaves has great practical significance. Here, fallen and yellow poplar leaves were used as the raw material, H₃PO₄ and KOH were used as activators, and urea was used as the nitrogen source to prepare ACs with abundant surface functional groups and pore structures. The pore structures and surface morphology, types and ratios of surface nitrogen- and oxygen-containing groups, and desorption features of the activated poplar leaves before and after urea treatment were characterized, and the adsorption and regeneration performance were also tested.

2. Results and Discussion

2.1. Characterization

(1) N₂ adsorption–desorption. The N₂ adsorption–desorption isotherms and pore size distribution curves for the H₃PO₄- and KOH-activated poplar leaves before and after N-doping are shown in Figure 1a,b, respectively. As shown in Figure 1a, in the initial stage of increasing partial pressure, the N₂ adsorption of the characterized ACs sharply increased, which is an indication of the existence of a large number of micropores [20,55]; as the relative pressure continuously increased, the N₂ adsorption slowly increased, and hysteresis loops appeared in the final stage, suggesting that mesopores also appeared in the activated poplar leaves [26,27]. In other words, both micropores and mesopores appeared in the poplar leaf-based ACs. From the pore size distribution curves in Figure 1b, the micropore size is mainly less than 1 nm, which is favourable for the physical adsorption of CO₂ [19,43]. The textural pore properties of the activated poplar leaves are shown in Table S1. As suggested in Table S1, the activated poplar leaves before and after N-doping had large specific surface areas and pore volumes ranging from 416–846 m²/g and 0.16–0.45 cm³/g, respectively. For H₃PO₄-activated poplar leaves, especially PH0.25N1, the pore properties, such as the specific surface area and pore volume, exhibited greater advantages than did those of KOH-activated poplar leaves.

(2) XPS spectrum. Based on previous research findings, the hydroxyl functional group of –OH, the ether functional groups of C–O and the pyrrolic nitrogen functional group of N–5 are favourable for CO₂ adsorption [41,50], so the O and N species, especially the ratios of –OH, C–O and N–5 in the prepared ACs, have received increased attention.

The XPS spectra for O1S and N1S of the H₃PO₄- and KOH-activated poplar leaves before and after N-doping are shown in Figures 2a–d and 2a'–d', respectively, and the peak area ratios of the O and N species are shown in Table S2 and Table S3, respectively. As shown in Figure 2a–d and Table S2, the total ratios of –OH and C–O for PH0.25 and PH0.25N1 are 11.04% and 10.21%, respectively, and the corresponding values for PK1 and PK1N1 are 24.47% and 18.74%, respectively; N-doping slightly reduces the amount of oxygen-containing functional groups, which may be caused by competition and interaction with nitrogen-containing functional groups. By comparison, the KOH-activated poplar leaves exhibited greater advantages in terms of oxygen-containing functional groups than the H₃PO₄-activated poplar leaves.

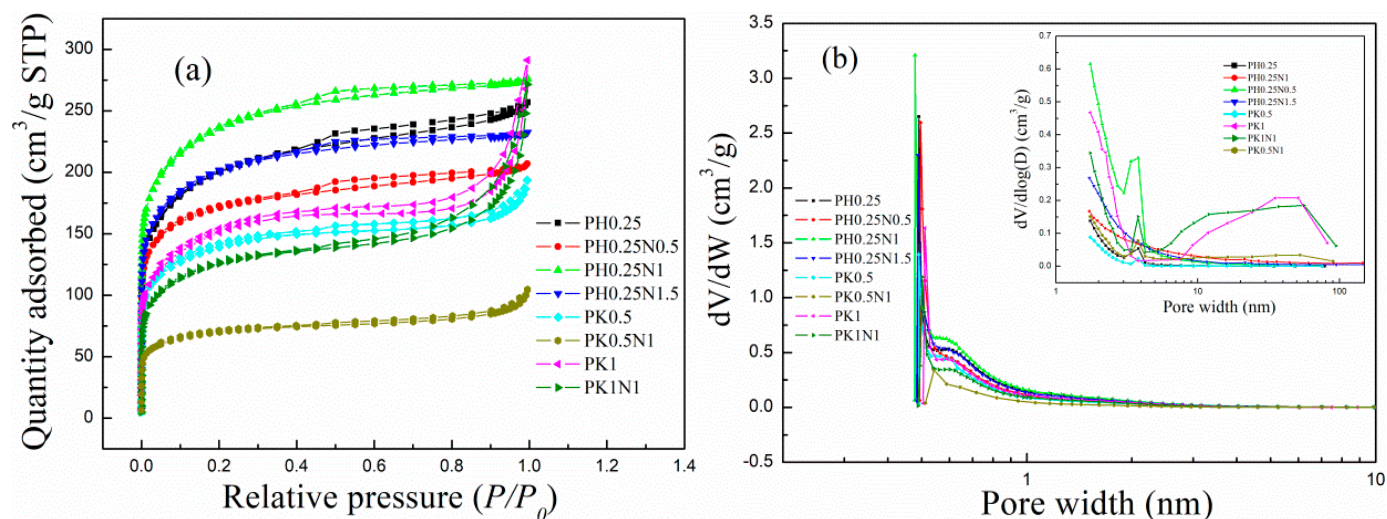


Figure 1. The (a) N₂ adsorption–desorption isotherms, and (b) pore size distribution curves of H₃PO₄– or KOH–activated poplar leaves before and after N-doping.

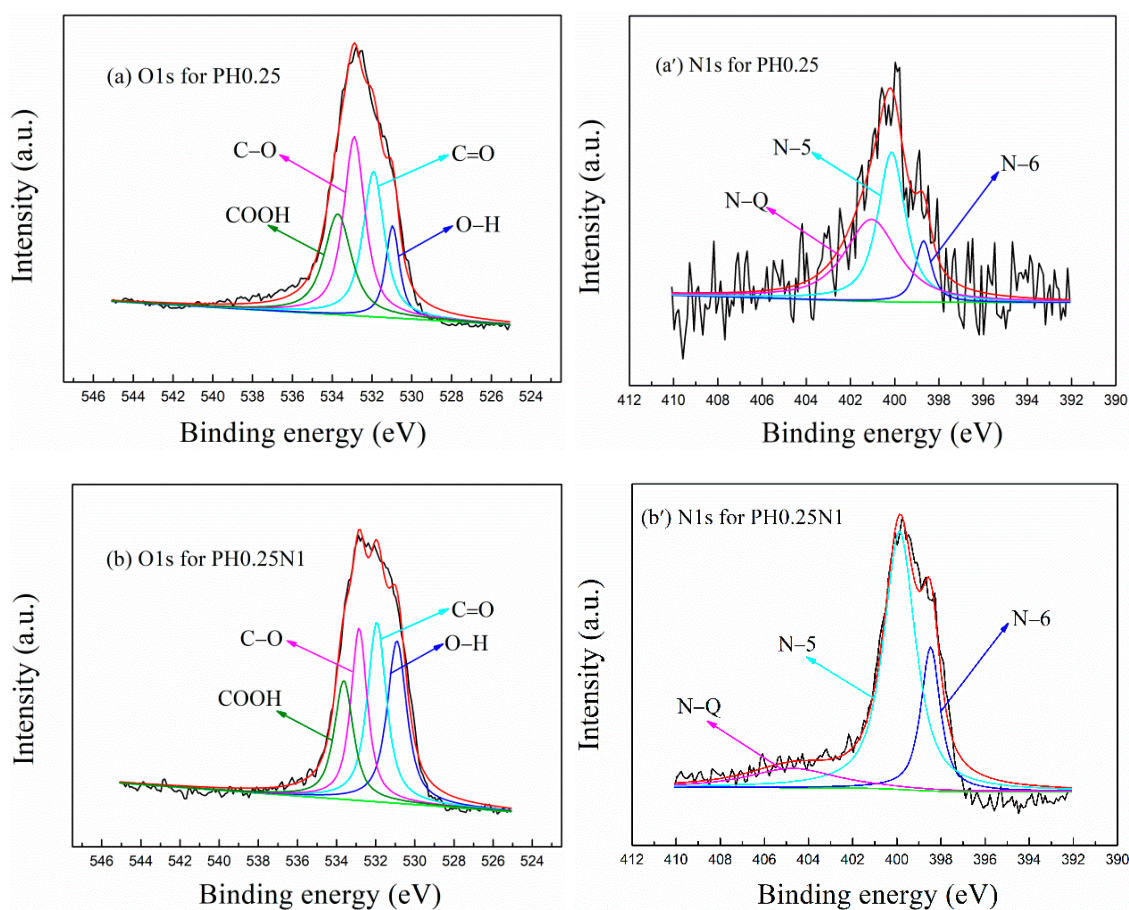


Figure 2. Cont.

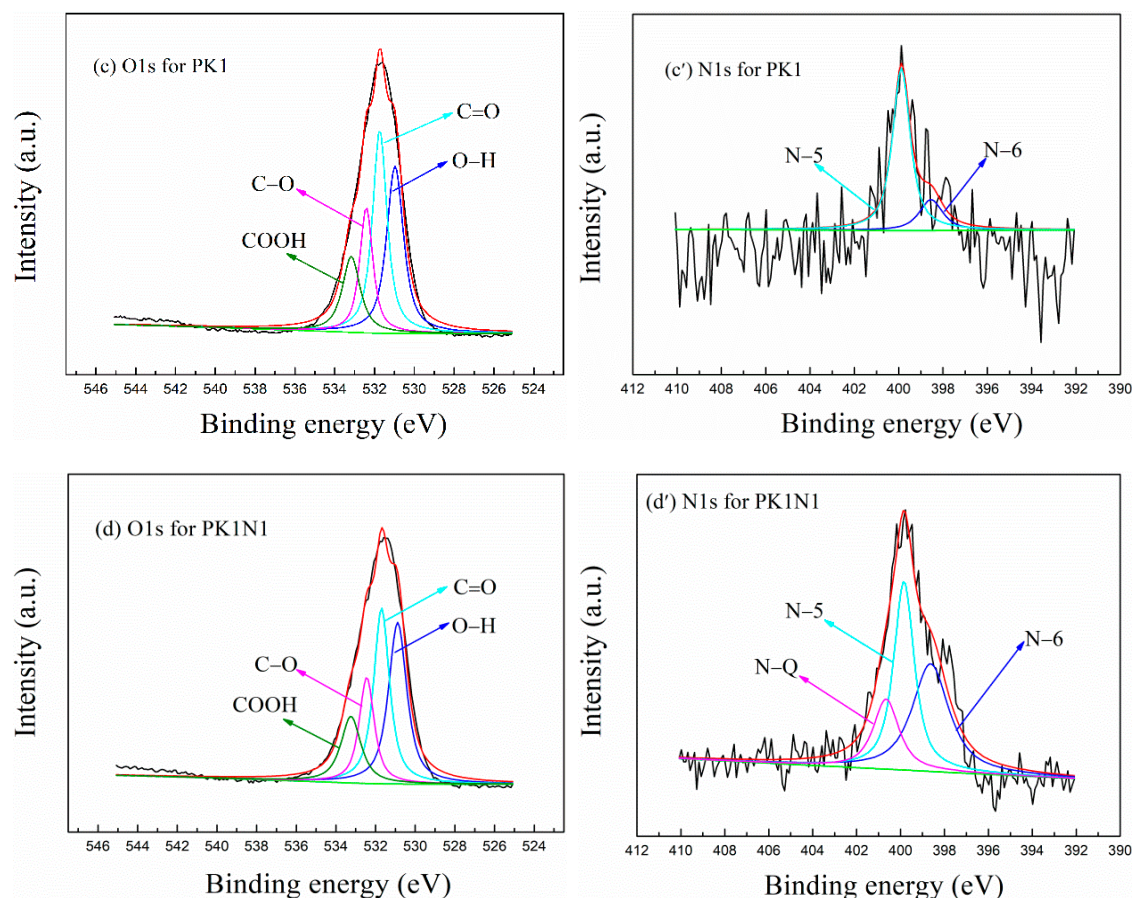


Figure 2. XPS spectra of H_3PO_4^- or KOH -activated poplar leaves before and after N-doping. (a–d): O1S, (a'–d'): N1S.

As shown in Figure 2a'–d' and Table S3, the ratios of N-5 for PH0.25 and PH0.25N1 are 0.96% and 6.38%, and the corresponding values for PK1 and PK1N1 are 2.09% and 1.58%, respectively. N-doping significantly increased the amount of nitrogen-containing functional groups on the H_3PO_4^- -activated poplar leaves, but slightly reduced the amount of KOH -activated poplar leaves, which may be caused by the strong corrosiveness of KOH or the competitive formation of quaternary nitrogen functional groups (N-Q).

(3) SEM

The surface morphology images of the H_3PO_4^- - and KOH -activated poplar leaves before and after N-doping are shown in Figure 3a–d. As shown in the Figures, the activation and N-doping of the poplar leaves led to the formation of developed and irregular pores. As shown in Figure 3a,b, the pores in PH0.25 are coarse and more developed and layered. As shown in Figure 3c,d, the KOH -activated poplar leaves formed dense and nearly circular pores, and after further N-doping, the pore surfaces were destroyed and became more disordered. By comparison, the surface morphology of the H_3PO_4^- -activated poplar leaves before and after N-doping was more suitable for CO_2 adsorption, and the characterization results were consistent with those of the BET characterization. The differences in the pore structure and surface morphology between H_3PO_4^- and KOH activation were mainly attributed to the activation mechanism and corrosiveness of H_3PO_4^- and KOH .

(4) CO_2 -TPD

The CO_2 -TPD curves for the H_3PO_4^- - and KOH -activated poplar leaves before and after N-doping are displayed in Figure 4a–d, which demonstrate the CO_2 desorption condition, and the initial adsorption temperature of the samples was set to 20°C . As shown in Figure 4, as the temperature increased, the desorption phenomenon gradually appeared and became obvious at relatively low temperatures, suggesting that the adsorption process

was mainly based on physisorption. However, the curve peaks for the studied sorbents all appeared at nearly 200 °C, which indicates that chemisorption was also involved in the adsorption process. The physisorption was mainly due to the narrow micropores and the hydrogen-bonding interactions between CO₂ and the O- or N-containing functional groups, and the chemisorption was mainly due to the reaction between the pyrrolic nitrogen functional groups and CO₂.

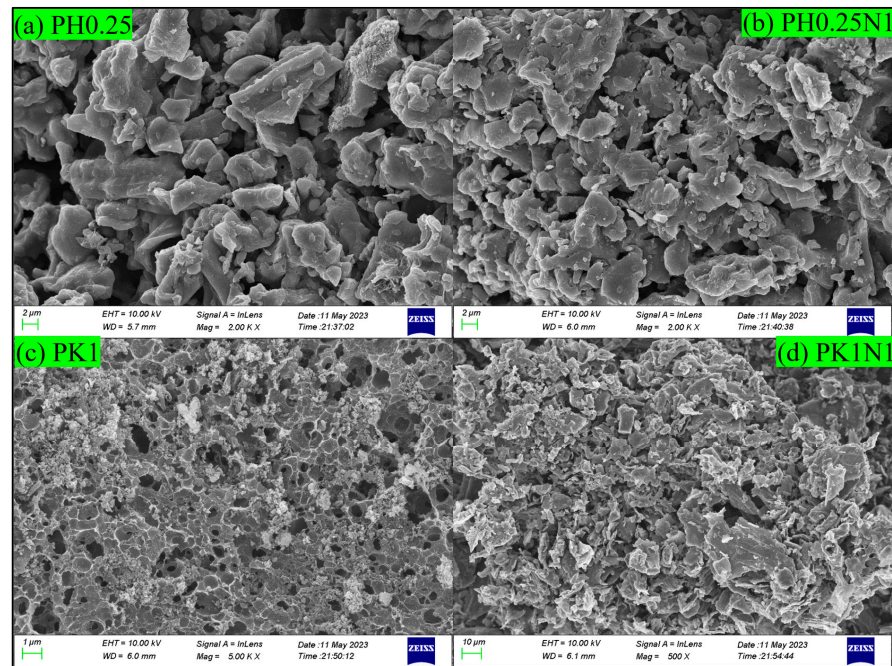


Figure 3. SEM images of H₃PO₄- or KOH-activated poplar leaves before and after N-doping.

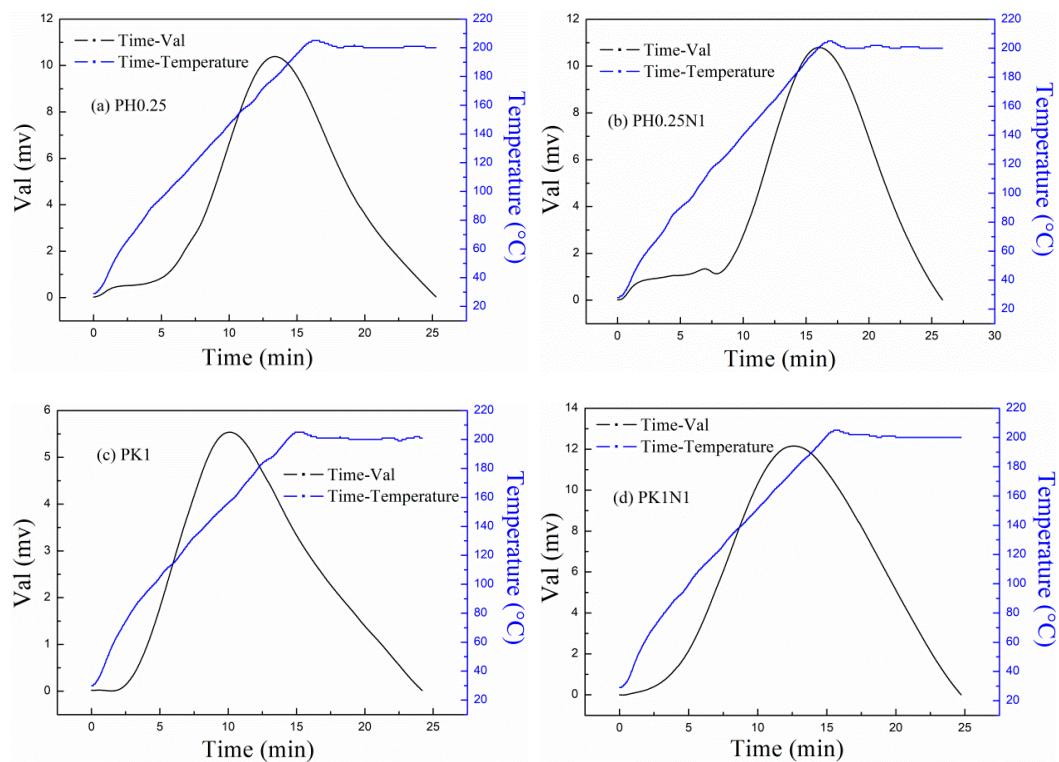


Figure 4. CO₂-TPD curves of H₃PO₄- or KOH-activated poplar leaves before and after N-doping.

For the N-doped sorbents, the desorption peaks appeared later than those of the H_3PO_4 - and KOH-activated poplar leaves, which was mainly caused by their stronger adsorption capacity and greater chemisorption.

2.2. CO_2 Adsorption Properties of Poplar Leaves-Based ACs

2.2.1. CO_2 Adsorption Performance and Process Optimization

Considering the factors that may affect the formation of pores and functional groups, the CO_2 adsorption performance of the ACs prepared with different volume ratios of H_3PO_4 to poplar leaves, mass ratios of KOH to poplar leaves, mass ratios of urea to H_3PO_4 , and KOH-activated poplar leaves were investigated, and the breakthrough adsorption curves and equilibrium adsorption capacities are shown in Figures 5a–e and 5a'–e', respectively.

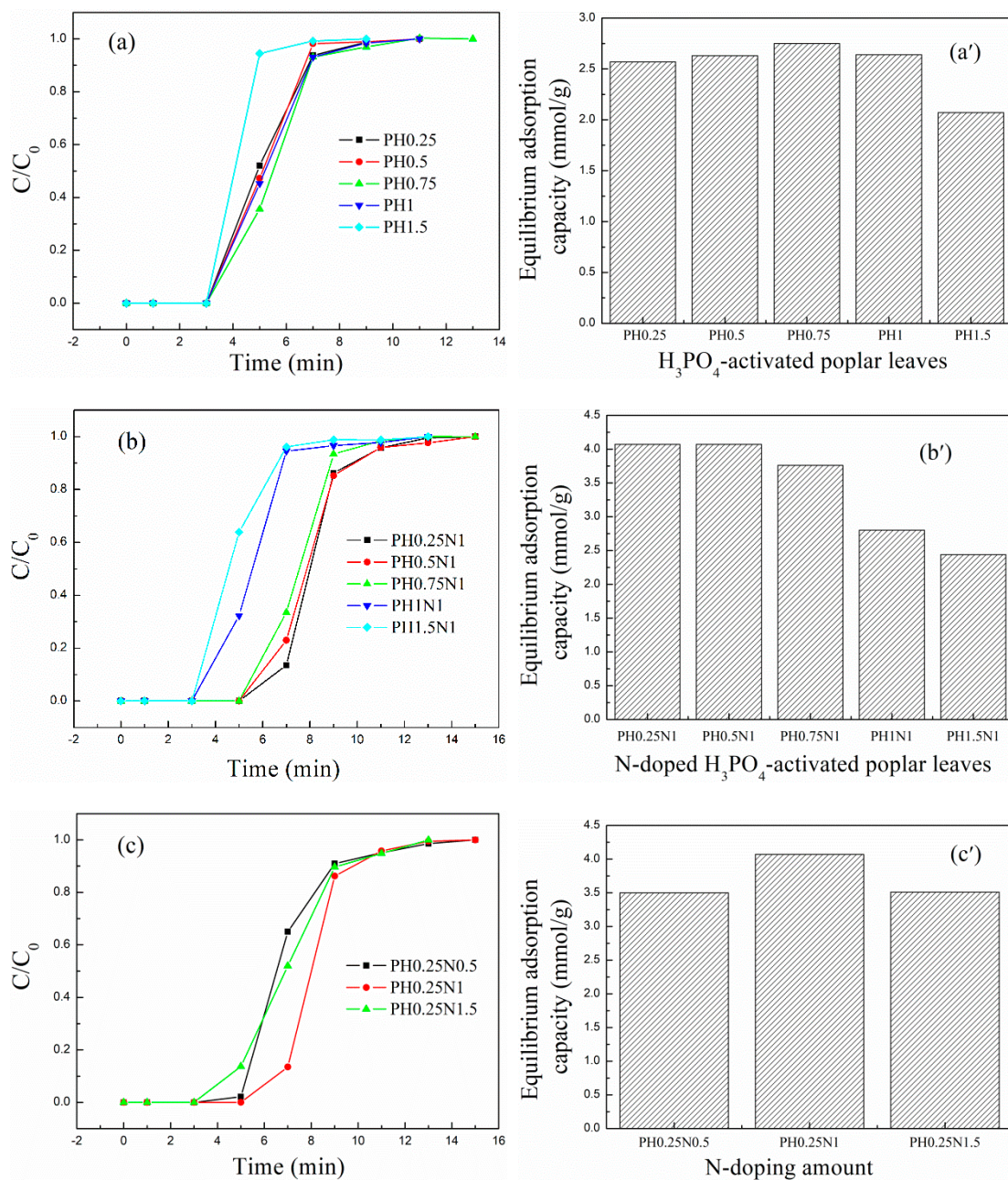


Figure 5. Cont.

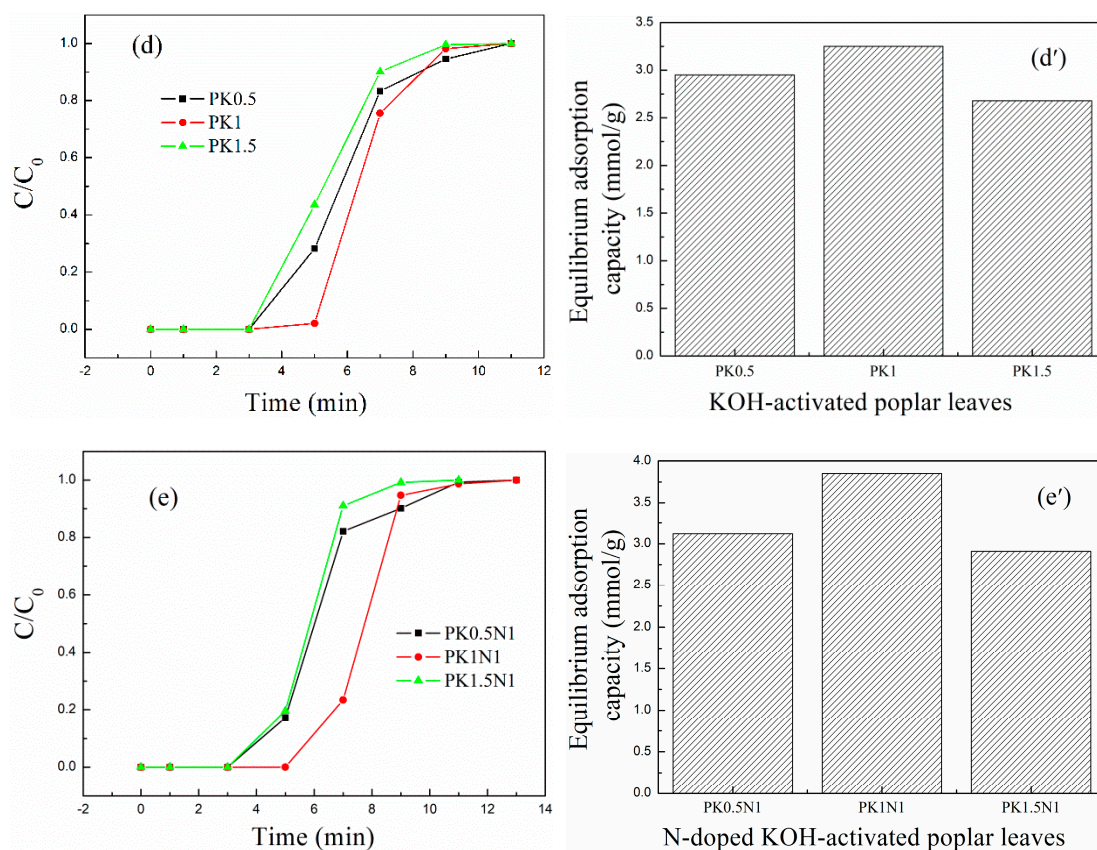


Figure 5. (a–e) CO_2 breakthrough adsorption curves and (a'–e') equilibrium adsorption capacities of H_3PO_4 - or KOH-activated poplar leaves before and after N-doping.

As shown in Figure 5a,b,a',b', as the volume ratio of H_3PO_4 to poplar leaves increased from 0.25 to 1, the equilibrium adsorption capacity of the H_3PO_4 -activated poplar leaves ranged between 2.57 and 2.74 mmol/g, which did not change much. However, as the ratio further increased to 1.5, the adsorption capacity decreased to 2.07 mmol/g. After further N-doping, with a 1:1 mass ratio of urea to H_3PO_4 -activated poplar leaves, the CO_2 adsorption capacity increased significantly compared with that of the H_3PO_4 -activated poplar leaves before N-doping; the CO_2 adsorption capacity ranged between 2.44 and 4.07 mmol/g, and exhibited a decreasing trend as the volume ratio of H_3PO_4 to poplar leaves increased. Considering both the preparation cost and the CO_2 adsorption capacity, the volume ratio of H_3PO_4 to poplar leaves was determined to be 0.25 to further investigate the effect of the N dopant amount.

The breakthrough adsorption curves and CO_2 adsorption capacities for different mass ratios of urea to PH0.25 are shown in Figures 5c and 5c', respectively. As the mass ratio increased from 0.5 to 1.5, the CO_2 adsorption performance first increased and then decreased, with a value of 4.07 mmol/g for the maximum PH0.25N1. In summary, when the volume ratio of H_3PO_4 to poplar leaves was 0.25:1 and the activation temperature was 450 °C, and the mass ratio of urea to H_3PO_4 -activated poplar leaves was 1:1 and the calcination temperature was 350 °C, the CO_2 adsorption performance for PH0.25N1 reached 4.07 mmol/g at 20 °C, which was comparable to the results of relative studies [41–44,49–52].

For KOH- and urea-modified poplar leaves, the adsorption performances are shown in Figure 5d,e and Figure 5d',e', respectively, and the N-doping treatment also increased the adsorption capacity of the KOH-activated poplar leaves. When the mass ratio of KOH to poplar leaves was 1:1 and the activation temperature was 700 °C, and the mass ratio of urea to PK1 was 1:1 and the calcination temperature was 350 °C, the CO_2 adsorption performance for PK1N1 reached 3.85 mmol/g at 20 °C, which was relatively lower than that of PH0.25N1.

In summary, from the view of material cost, corrosiveness, process energy consumption, and adsorption performance, H_3PO_4 has more advantages than KOH as an activator of poplar leaves.

2.2.2. The Adsorption Kinetics of the Poplar Leaf-Based ACs

Adsorption kinetics are also important indices for evaluating the adsorption properties of an adsorbent. The pseudo-first-order, pseudo-second-order and Avrami models were used to simulate the adsorption kinetics of H_3PO_4 - and KOH -activated poplar leaves before and after N-doping. The fitting curves are shown in Figure 6, and the fitting parameters are shown in Table 1. From the fitting results, only the Avrami model was well fitted to the experimental adsorption capacities of PH0.25, PH0.25N1, PK1, and PK1N1. The variance in R^2 ranged between 0.9948 and 0.9982, and n_a ranged between 1.4272 and 1.5571, suggesting that the Avrami model is more suitable for describing the adsorption kinetics of poplar leaf-based ACs than the pseudo-first-order and pseudo-second-order models. Adsorption involves not only physisorption or chemisorption, but also a comprehensive adsorption process [27,28,33].

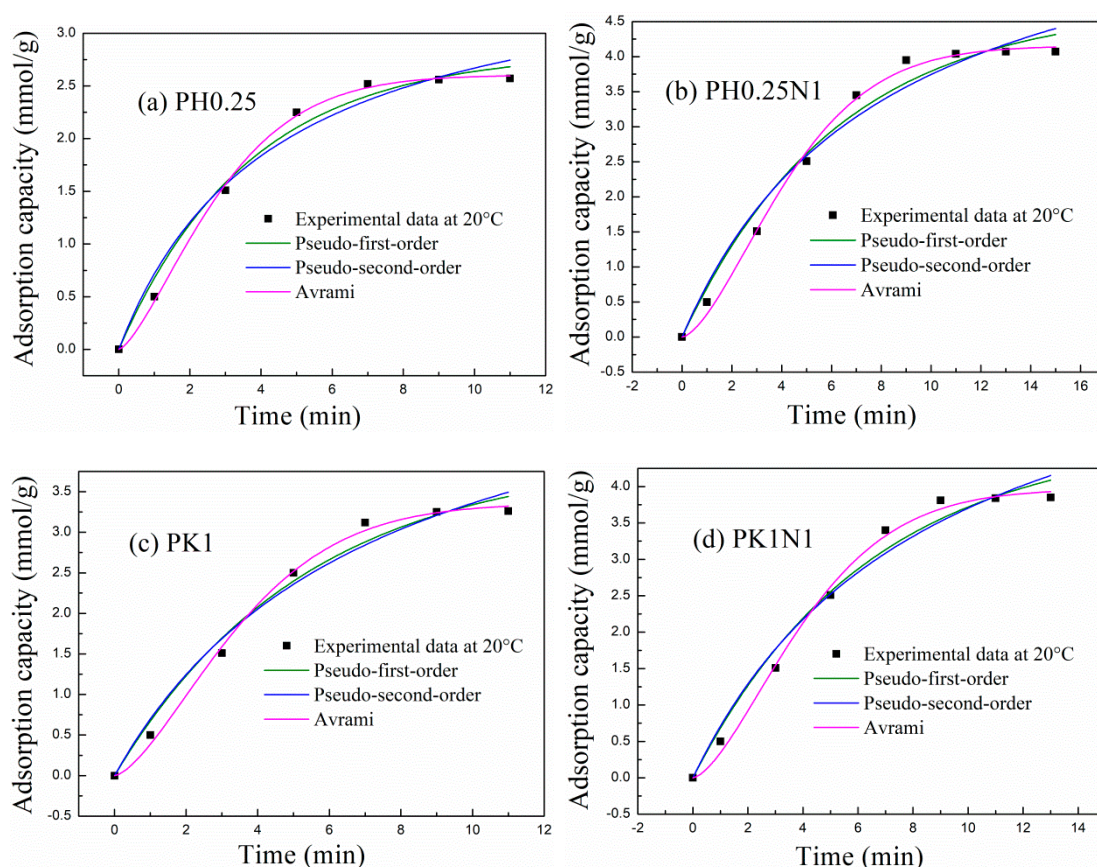


Figure 6. Nonlinear fitting curves of the experimental adsorption data of H_3PO_4 - or KOH -activated poplar leaves before and after N-doping according to different kinetic models.

For PH0.25 and PH0.25N1, the adsorption rate constants are 0.3146 and 0.2016 min^{-1} , respectively, while they are 0.2485 and 0.2108 min^{-1} for PK1 and PK1N1, respectively. For the H_3PO_4 - and KOH -activated poplar leaves after N-doping, the adsorption rate constants all decreased, which corresponded with decreased adsorption rates. Combined with the above mentioned XPS characterization, these findings indicate that N-doping results in more N- and O-containing functional groups, which promote more chemisorption during the adsorption process, and that the adsorption rate decreases.

Table 1. Nonlinear fitting parameters of the experimental adsorption data of H₃PO₄- or KOH-activated poplar leaves before and after N-doping according to different kinetic models.

Kinetic Model	Parameter	PN0.25	PN0.25N1	PK1	PK1N1
Pseudo -first-order	q_e (mmol/g)	2.82	4.74	3.94	4.69
	k_1 (1/min)	0.2741	0.1610	0.1872	0.1572
	R^2	0.9854	0.9789	0.9821	0.9802
Pseudo -second-order	q_e (mmol/g)	3.83	6.78	5.83	6.97
	k_2 (g/mmol min)	0.0602	0.0182	0.0233	0.0163
	R^2	0.9744	0.9704	0.9759	0.9739
Avrami	q_e (mmol/g)	2.60	4.15	3.36	3.96
	k_a (1/min)	0.3146	0.2016	0.2485	0.2108
	n_a	1.4272	1.5571	1.5093	1.5410
	R^2	0.9982	0.9955	0.9955	0.9948

The adsorption data were further treated with the intraparticle diffusion model, and the fitting results are shown in Figure S1. From the fitting results, the third adsorption stage had the smallest slope of 0.14, suggesting that the equilibrium adsorption stage was the rate-controlling step, and the boundary layer diffusion and intraparticle diffusion stages were quick.

2.2.3. The Adsorption Thermodynamics of the Poplar Leaves-Based ACs

In view of the high adsorption capacity, PH0.25N1 was selected to further investigate the adsorption thermodynamic characteristics. The adsorption temperature and CO₂ partial pressure were set as 20–40 °C and 0–15 kPa, respectively. The Langmuir adsorption isotherm equation was used to fit the experimental adsorption data, and the Clausius–Clapyron equation was used to calculate the isosteric heat of adsorption. Corresponding fittings are shown in Figure 7a,b, and the fitting parameters are shown in Table 2. As shown in Figure 7a and Table 2, the experimental data showed good fitting with the Langmuir equation, in which R^2 ranged above 0.99, showing that the Langmuir model could describe the adsorption characteristic of PH0.25N1. In addition, the experimental data suggested good linear fitting with the Clausius–Clapyron equation, and the calculated isosteric heat of adsorption was almost 28 kJ/mol when the adsorption capacity ranged from 0.6 to 1.8 mmol/g, which is an indication that the adsorption of PH0.25N1 was mainly physisorption. As the adsorption temperature increased from 20 to 40 °C, the value of k_L gradually decreased from 0.01316 to 0.00874, which is also a physisorption characteristic.

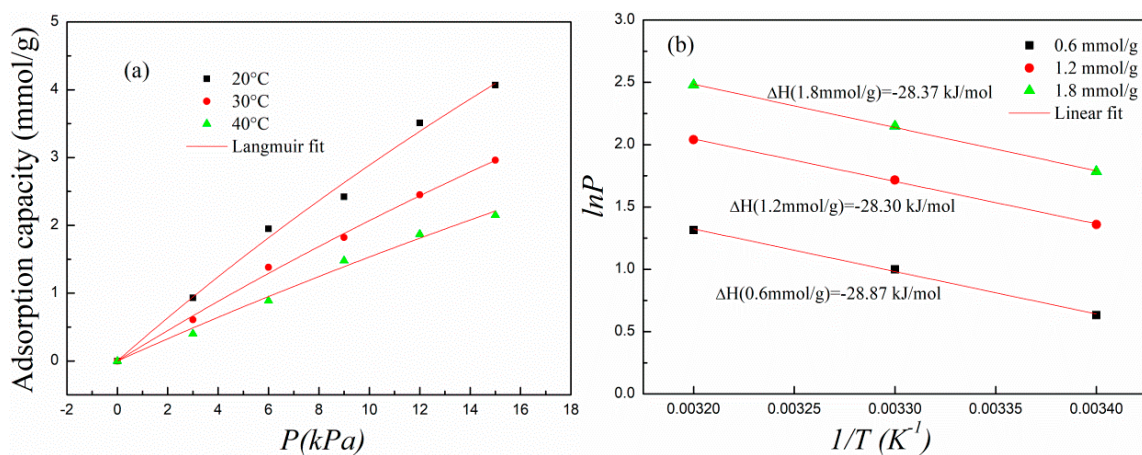
**Figure 7.** (a) Nonlinear fitting of the experimental adsorption data of PH0.25N1 with Langmuir model and (b) linear fitting with Clausius–Clapyron equation.

Table 2. Nonlinear fitting parameters of PH0.25N1 according to the Langmuir model.

Parameter	20 °C	30 °C	40 °C
The fitting equilibrium adsorption capacity (mmol/g)	24.84	21.23	19.07
k_L	0.01316	0.0108	0.00874
R^2	0.9918	0.9970	0.9908

2.2.4. Linear Correlation Analysis between the Adsorption Capacity and Influencing Factors

The surface functional groups, specific surface areas, and total pore volume, especially the micropore volume, largely determine the adsorption performance of adsorbents [51]. In view of the good adsorption performance of PH0.25, PH0.25N1, PK1, and PK1N1, they were selected to study the dependence of adsorption capacity on the influencing factors, and the linear correlation fittings are shown in Figure 8. The fitting Figures indicate that the adsorption capacity did not show a good but rather a relatively weak correlation with the content of the N-5 groups, the total pore volume, the micropore volume, and the specific surface area, suggesting that none of the above factors played a decisive role in the adsorption of the poplar leaf-based ACs, but rather had a comprehensive impact.

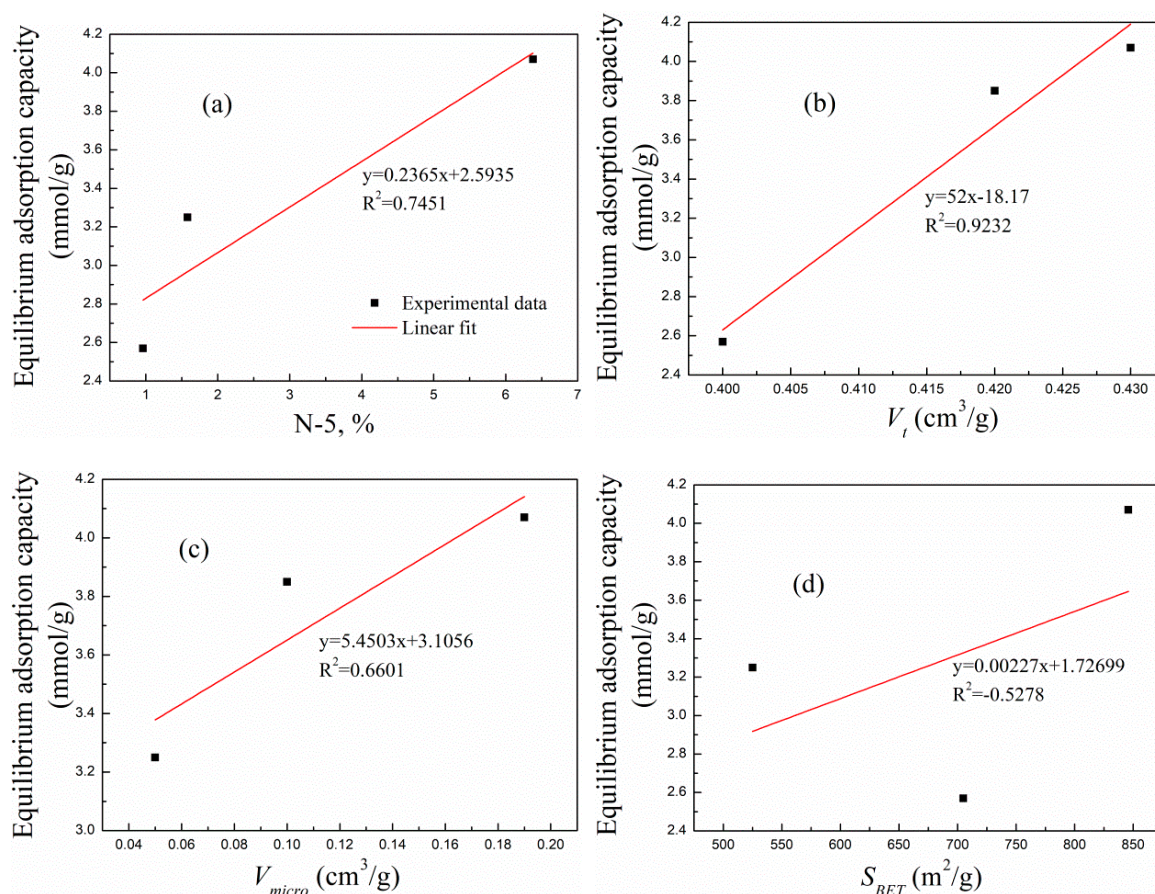


Figure 8. Linear fitting of the equilibrium adsorption capacity of the prepared ACs with relevant parameters. (a) The ratio of N-5 functional groups, (b) V_t , (c) V_{micro} , and (d) S_{BET} .

2.3. The Regeneration Performance of the Selected ACs

In view of their good adsorption performance, PH0.25N1 and PK1N1 were selected for further investigation of their regeneration performance. The adsorption temperature was 20 °C and the regeneration temperature was set to 200 °C according to the CO₂-TPD results. The adsorption capacities after every regeneration for both samples are exhibited in

Figure 9. As shown in Figure 9, the adsorption capacities of PH0.25N1 and PK1N1 exhibited slight decreases during the ten regeneration cycles—3.95 and 3.70 mmol/g after the tenth regeneration, and were reduced by only 2.95 and 3.90%, respectively, compared with that of the fresh samples. The regeneration performance of the poplar leaf-based ACs was comparable to that reported in the related literature [30,33,50,51].

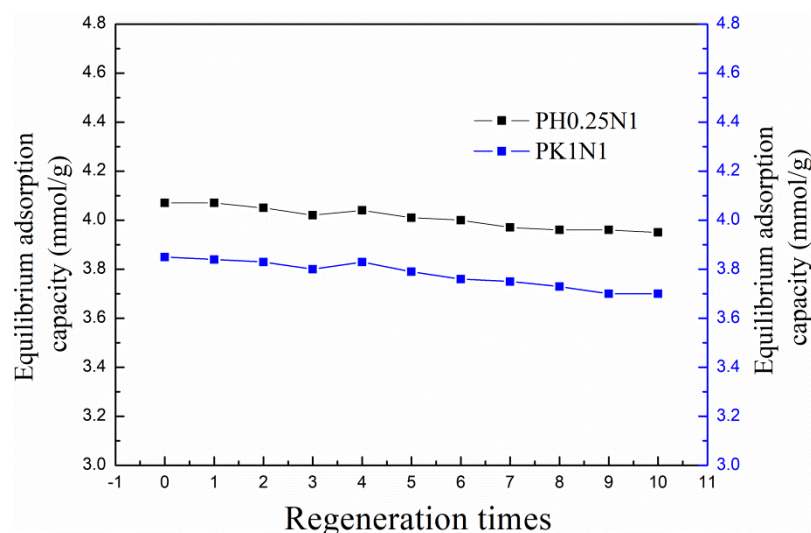


Figure 9. The equilibrium adsorption capacities of PH0.25N1 and PK1N1 after regeneration.

Table 3 describes the adsorption and regeneration performance of biomass-based ACs both in the literature and this work. As shown in Table 3, both the adsorption and regeneration performance of the poplar leaf-based ACs were comparable with those in the related work.

Table 3. The equilibrium adsorption capacity (q_e) of the fresh and regenerated biomass-based ACs.

Sorbent	q_e (mmol/g) of Fresh Sample	q_e (mmol/g) of Sample after Ten Regenerations	Condition	Reference
SCK-800-1	1.05	0.91	25 °C, 18% CO ₂ + 82% N ₂	[37]
CK0.3-700(1)	3.49	3.44	20 °C, 15% CO ₂ + 85% N ₂	[50]
CN1K0.3-700(1)	4.58	4.52	20 °C, 15% CO ₂ + 85% N ₂	[50]
PAC-0.5K2CO3-750-0.5	2.41	2.38	20 °C, 15% CO ₂ + 85% N ₂	[51]
PK1N1	3.85	3.70	20 °C, 15% CO ₂ + 85% N ₂	This work
PH0.25N1	4.07	3.95	20 °C, 15% CO ₂ + 85% N ₂	This work

3. Materials and Methods

3.1. Materials

Poplar leaves were collected from the campus of Weifang University in Shandong, China. H₃PO₄ (AR, 85%) was purchased from Tianjin Kemio Chemical Reagent Co., Ltd., in Tianjin, China. KOH (GR, 85%) and urea (AR, 99%) were purchased from Shanghai Aladdin Biochemical Technology Co., Ltd., in Shanghai, China.

N₂ (99.999%) and the simulated flue gas (85 vol.% N₂ + 15 vol.% CO₂) were obtained from Weiyang Gas Co., Ltd., in Yantai, China.

3.2. Preparation of Poplar Leaf-Based ACs

Poplar leaves were first washed with tap water and subsequently with distilled water, and then were subsequently dried in a heating oven at 80 °C. The leaves were subsequently ground into powder and sieved to less than 80 mesh for backup. Flaky KOH was also ground into powder for use.

3.2.1. H₃PO₄- and KOH-Activated Poplar Leaves

A certain volume of H₃PO₄ (10.5, 21, 31.5, 42 mL) was slowly poured into a beaker containing a certain volume of dried poplar leaves (20 g, 42 mL), during which continuous stirring with a glass rod was used to process the leaves evenly soaked in H₃PO₄, after which the beaker was left to stand for 6 h. Subsequently, the mixture was dried at 120 °C, calcined in a muffle furnace for 1 h at 450 °C under an Ar atmosphere, washed with distilled water, and dried at 100 °C. The obtained black powder is denoted as PHa, in which P and H are poplar leaves and H₃PO₄, respectively, and a is the volume ratio of H₃PO₄ to poplar leaves. The final weight of PHa was 9.02–10.16 g, and the yield was 45.1–50.8%.

In the same way, KOH-activated poplar leaves were also prepared. However, KOH and P were mixed according to a mass ratio rather than a volume ratio, and the calcination temperature was set to 700 °C. The obtained black powder was denoted as PKc, in which K was KOH and c was the mass ratio of KOH to P, with the value of c ranging from 0.5 to 1.5. The yield of PKc was 40.7–46.2%.

3.2.2. N-doping PHa and PKc

A certain mass ratio of urea to PHa or PKc was uniformly mixed and then calcined in a muffle furnace for 2 h at 350 °C under an Ar atmosphere. The mixture was subsequently washed with distilled water and dried at 100 °C. The obtained black powders were tracked as PHaNb and PKcNd, where N represents urea and b and d are the mass ratios of urea to PHa and PKc, respectively, with the value ranging from 0.5 to 1.5. The yield (the weight of the product divide by the weight of PHa or PKc) of PHaNb and PKcNd were 80–95%.

3.3. Characterization

The pore structures of the poplar leaf-based ACs were characterized on an ASAP 2460 (Micromeritics, Irvine, CA, USA) by the physical adsorption of N₂ at a critical temperature of −196 °C. The BET specific surface area of S_{BET} was obtained according to the Brunauer–Emmett–Teller (BET) equation, the total pore volume V_t was calculated from the N₂ adsorption amount as the relative pressure of P/P₀ was 0.996, the micropore volume V_{micro} was obtained according to the t-plot curves, and the pore size distribution was obtained from the desorption branch according to the density functional theory method and BJH method.

X-ray photoelectron spectroscopy (XPS) characterization was performed on an EscaLab 250Xi (Thermo Scientific, Waltham, MA, USA), and the functional group ratios of N and O species were determined according to the XPS spectra.

Scanning electron microscopy (SEM) characterization of the poplar leaf-based ACs was performed on a JSM-7500F scanning electron microscope (JEOL, Showa City, Tokyo, Japan) at 5.0 kV, and surface morphology images were collected.

CO₂ temperature-programmed desorption (TPD) characterization was also performed on a TP-5080 (Xianquan, Tianjin, China). The heating rate was 1 °C/min, and the maximum temperature was 200 °C.

3.4. Adsorption and Regeneration

CO₂ adsorption and regeneration experiments were conducted on a self-assembled fixed-bed reactor. The inner diameter of the quartz loading tube is 0.8 cm, and the wall thickness is 0.1 cm. The gas chromatograph was connected at the outlet of the reactor, and the CO₂ concentration was recorded. Firstly, 0.4 g of the ACs was laid flat in a quartz tube, N₂ was introduced to purge the adsorbed CO₂ and H₂O, etc., and the reactor was adjusted to the predetermined adsorption temperature. Here, N₂ was transferred to the simulated flue gas, after which the adsorption process began. C₀ and C represent the CO₂ concentrations at the inlet and outlet of the reactor, respectively. As adsorption proceeded, C gradually increased to C₀, which indicated that the CO₂ adsorption process reached equilibrium. The inlet gas was then retransferred to N₂, and the reactor temperature was adjusted to 200 °C to regenerate the saturated sample. When the outlet concentration of C

gradually decreased to 0, the sorbent was completely regenerated, and the regeneration process was complete.

4. Conclusions

Fluttered poplar leaves were used to prepare ACs with abundant pore structures and N- and O-containing functional groups using H_3PO_4 or KOH activation and nitrogen doping methods for CO_2 capture. When the volume ratio of H_3PO_4 to poplar leaves was 0.25:1 and the activation temperature was $450\text{ }^\circ\text{C}$, and the mass ratio of urea to H_3PO_4 -activated poplar leaves was 1:1 and the calcination temperature was $350\text{ }^\circ\text{C}$, the equilibrium CO_2 adsorption capacity for PH0.25N1 was 4.07 mmol/g at $20\text{ }^\circ\text{C}$. Similarly, when the mass ratio of KOH to poplar leaves was 1:1 and the activation temperature was $700\text{ }^\circ\text{C}$, and the mass ratio of urea to PK1 was 1:1 and the calcination temperature was $350\text{ }^\circ\text{C}$, the CO_2 adsorption capacity for PK1N1 was 3.85 mmol/g at $20\text{ }^\circ\text{C}$. The CO_2 -TPD characterization, adsorption kinetics, and linear correlation results showed that the adsorption process involved both physisorption and chemisorption, and the content of the N-5 groups, the total and the micro pore volume, and the specific surface area had comprehensive impacts on the CO_2 adsorption of the poplar leaf-based ACs. The calculated isosteric heat of adsorption was almost 28 kJ/mol when the adsorption capacity ranged from 0.6 to 1.8 mmol/g , which is an indication that the adsorption of PH0.25N1 was mainly physisorption; the equilibrium adsorption stage was the rate-controlling step. In addition, the selected ACs PH0.25N1 and PK1N1 showed good regeneration performance, with adsorption capacities reducing by 2.95 and 3.90%, respectively, after ten regenerations. By comprehensively considering the material cost, corrosiveness, process energy consumption and adsorption performance, H_3PO_4 has more advantages than KOH as an activator of poplar leaves.

As waste biomass, poplar leaves are utilized as a source raw material for preparing ACs for CO_2 capture, and the preparation process involves low energy consumption. The prepared poplar leaf-based ACs are excellent CO_2 sorbents with potential applications.

Supplementary Materials: The following supporting information can be downloaded at: <https://www.mdpi.com/article/10.3390/molecules29092024/s1>. Figure S1: The prediction of the rate-controlling step of PH0.25N1 by the intraparticle diffusion model; Table S1: The textural pore properties of H_3PO_4 - or KOH-activated poplar leaves before and after N-doping; Table S2: The peak area ratios of the O species in H_3PO_4 - or KOH-activated poplar leaves before and after N-doping; Table S3: The peak area ratios of the N species in H_3PO_4 - or KOH-activated poplar leaves before and after N-doping.

Author Contributions: Conceptualization, F.K.; Data curation, W.Z. and C.X.; Funding acquisition, F.K.; Investigation, F.K.; Methodology, X.W. and C.X.; Project administration, X.W. and X.K.; Resources, H.Z.; Software, W.Z.; Supervision, X.W.; Validation, H.Z. and X.K.; Writing—original draft, W.Z.; Writing—review and editing, H.Z. All authors have read and agreed to the published version of the manuscript.

Funding: The financial support from the National Natural Science Foundation of China (Grant No. 22108208), the State Key Laboratory of High-efficiency Utilization of Coal and Green Chemical Engineering (Grant No. 2021-K02) and Shandong Province Science and Technology Small and Medium sized Enterprise Innovation Ability Enhancement Project (Grant No. 2023TSGC0776) is gratefully acknowledged.

Institutional Review Board Statement: Not applicable.

Informed Consent Statement: Not applicable.

Data Availability Statement: The data that support the findings of this study are available from the corresponding author, X. Wang, upon reasonable request.

Conflicts of Interest: The authors declare no conflicts of interest.

References

1. Boot-Handford, M.E.; Abanades, J.C.; Anthony, E.J.; Blunt, M.J.; Brandani, S.; Dowell, N.M.; Fernandez, J.R.; Ferrari, M.-C.; Gross, R.; Hallett, J.P. Carbon capture and storage update. *Energy Environ. Sci.* **2014**, *7*, 130–189. [[CrossRef](#)]
2. Sevilla, M.; Fuertes, A.B. Sustainable porous carbons with a superior performance for CO₂ capture. *Energy Environ. Sci.* **2011**, *4*, 1765–1771. [[CrossRef](#)]
3. Mai, B.; Adjiman, C.S.; Bardow, A.; Anthony, E.J.; Dowell, N.M. Carbon capture and storage (CCS): The way forward. *Energy Environ. Sci.* **2018**, *11*, 1062–1176.
4. Bhowan, A.S.; Freeman, B.C. Analysis and status of post combustion carbon dioxide capture technologies. *Environ. Sci. Technol.* **2011**, *45*, 8624–8632. [[CrossRef](#)]
5. Hussain, M.A.; Soujanya, Y.; Sastry, G.N. Evaluating the efficacy of amino acids as CO₂ capturing agents: A first principles investigation. *Environ. Sci. Technol.* **2011**, *45*, 8582–8588. [[CrossRef](#)]
6. Rayer, A.V.; Mobley, P.D.; Soukri, M.; Gohndrone, T.R.; Tanthana, J.; Zhou, J.; Lail, M. Absorption rates of carbon dioxide in amines in hydrophilic and hydrophobic solvents. *Chem. Eng. J.* **2018**, *348*, 514–525. [[CrossRef](#)]
7. Samanta, A.; Bandyopadhyay, S.S. Absorption of carbon dioxide into aqueous solutions of piperazine activated 2-amino-2-methyl-1-propanol. *Chem. Eng. Sci.* **2009**, *64*, 1185–1194. [[CrossRef](#)]
8. Hwang, S.J.; Lee, M.; Kim, H.; Lee, K.S. Cyclic CO₂ absorption capacity of aqueous single and blended amine solvents. *J. Ind. Eng. Chem.* **2018**, *65*, 95–103. [[CrossRef](#)]
9. Yang, S.-T.; Kim, J.-Y.; Kim, J.; Ahn, W.-S. CO₂ capture over amine-functionalized MCM-22, MCM-36 and ITQ-2. *Fuel* **2012**, *97*, 435–442. [[CrossRef](#)]
10. Samanta, A.; Zhao, A.; Shimizu, G.K.H.; Sarkar, P.; Gupta, R. Post-combustion CO₂ capture using solid sorbents: A review. *Ind. Eng. Chem. Res.* **2012**, *51*, 1438–1463. [[CrossRef](#)]
11. Xiao, J.; Sitamraju, S.; Janik, M.J. CO₂ adsorption thermodynamics over N-substituted/grafted graphanes: A DFT study. *Langmuir* **2014**, *30*, 1837–1844. [[CrossRef](#)] [[PubMed](#)]
12. Muriithi, G.N.; Petrik, L.F.; Doucet, F.J. Synthesis, characterization and CO₂ adsorption potential of NaA and NaX zeolites and hydrotalcite obtained from the same coal fly ash. *J. CO₂ Util.* **2020**, *36*, 220–230. [[CrossRef](#)]
13. Aquino, T.F.D.; Estevam, S.T.; Viola, V.O.; Marques, C.R.M.; Zancan, F.L.; Vasconcelos, L.B.; Riella, H.G.; Pires, M.J.R.; Morales-Ospino, R.; Torres, A.E.B.; et al. CO₂ adsorption capacity of zeolites synthesized from coal fly ashes. *Fuel* **2020**, *276*, 118143–118152. [[CrossRef](#)]
14. Zhang, J.; Huang, D.; Shao, J.; Zhang, X.; Zhang, S.; Yang, H.; Chen, H. A new nitrogen-enriched biochar modified by ZIF-8 grafting and annealing for enhancing CO₂ adsorption. *Fuel Process. Technol.* **2022**, *231*, 107250–107259. [[CrossRef](#)]
15. Tuci, G.; Iemhoff, A.; Rossin, A.; Yakhvarov, D.; Gatto, M.F.; Balderas-Xicohtencatl, R.; Zhang, R.; Hirscher, M.; Palkovits, R.; Pham-Huu, C.; et al. Tailoring morphological and chemical properties of covalent triazine frameworks for dual CO₂ and H₂ adsorption. *Int. J. Hydrogen Energy* **2022**, *47*, 8434–8445. [[CrossRef](#)]
16. Chang, C.-W.; Kao, Y.-H.; Shen, P.-H.; Kang, P.-C.; Wang, C.-Y. Nanoconfinement of metal oxide MgO and ZnO in zeolitic imidazolate framework ZIF-8 for CO₂ adsorption and regeneration. *J. Hazard. Mater.* **2020**, *400*, 122974–122986. [[CrossRef](#)]
17. Martell, J.D.; Milner, P.J.; Siegelman, R.L.; Long, J.R. Kinetics of cooperative CO₂ adsorption in diamine-appended variants of the metal-organic framework Mg₂(dobpdc). *Chem. Sci.* **2020**, *11*, 6457–6471. [[CrossRef](#)] [[PubMed](#)]
18. Lourenço, M.A.O.; Fontana, M.; Jagdale, P.; Pirri, C.F.; Bocchini, S. Improved CO₂ adsorption properties through amine functionalization of multi-walled carbon nanotubes. *Chem. Eng. J.* **2021**, *414*, 128763–128775. [[CrossRef](#)]
19. Wang, X.; Zeng, W.; Liu, W.; Cao, X.; Hou, C.; Ding, Q.; Lu, Y. CO₂ adsorption of lignite chars after one-step activation. *New J. Chem.* **2020**, *44*, 13755–13763. [[CrossRef](#)]
20. Yi, H.; Li, F.; Ning, P.; Tang, X.; Peng, J.; Li, Y.; Deng, H. Adsorption separation of CO₂, CH₄, and N₂ on microwave activated carbon. *Chem. Eng. J.* **2013**, *215–216*, 635–642.
21. Arami-Niya, A.; Rufford, T.E.; Zhu, Z. Activated carbon monoliths with hierarchical pore structure from tar pitch and coal powder for the adsorption of CO₂, CH₄ and N₂. *Carbon* **2016**, *103*, 115–124. [[CrossRef](#)]
22. Meng, M.; Qiu, Z.; Zhong, R.; Liu, Z.; Liu, Y.; Chen, P. Adsorption characteristics of supercritical CO₂/CH₄ on different types of coal and a machine learning approach. *Chem. Eng. J.* **2019**, *368*, 847–864. [[CrossRef](#)]
23. Wang, J.; Kaskel, S. KOH activation of carbon-based materials for energy storage. *J. Mater. Chem.* **2012**, *22*, 23710–23725. [[CrossRef](#)]
24. Mafra, L.; Čendak, T.; Schneider, S.; Wiper, P.V.; Pires, J.; Gomes, J.R.B.; Pinto, M.L. Amine functionalized porous silica for CO₂/CH₄ separation by adsorption: Which amine and why. *Chem. Eng. J.* **2018**, *336*, 612–621. [[CrossRef](#)]
25. Liu, X.; Yang, X.; Du, H.; Wu, Y.; Zhang, X.; Zhang, J. Preparation and characterization of a porous silicate material using a CO₂-storage material for CO₂ adsorption. *Powder Technol.* **2018**, *333*, 138–152. [[CrossRef](#)]
26. Wang, Y.; Hu, X.; Guo, T.; Tian, W.; Hao, J.; Guo, Q. The competitive adsorption mechanism of CO₂, H₂O and O₂ on a solid amine adsorbent. *Chem. Eng. J.* **2021**, *416*, 129007–129017. [[CrossRef](#)]
27. Wang, X.; Zeng, W.; Song, M.; Wang, F.; Hu, X.; Guo, Q.; Liu, Y. Polyetheramine improves the CO₂ adsorption behavior of tetraethylenepentamine-functionalized sorbents. *Chem. Eng. J.* **2019**, *364*, 475–484. [[CrossRef](#)]

28. Wang, Y.; Hu, X.; Hao, J.; Ma, R.; Guo, Q.; Gao, H.; Bai, H. Nitrogen and oxygen codoped porous carbon with superior CO₂ adsorption performance: A combined experimental and DFT calculation study. *Ind. Eng. Chem. Res.* **2019**, *58*, 13390–13400. [[CrossRef](#)]
29. Kuwahara, Y.; Hanaki, A.; Yamashita, H. A direct conversion of blast furnace slag to a mesoporous silica-calcium oxide composite and its application in CO₂ captures. *Green Chem.* **2020**, *22*, 3759–3768. [[CrossRef](#)]
30. Wang, Y.; Guo, T.; Hu, X.; Hao, J.; Guo, Q. Mechanism and kinetics of CO₂ adsorption for TEPA-impregnated hierarchical mesoporous carbon in the presence of water vapor. *Powder Technol.* **2020**, *368*, 227–236. [[CrossRef](#)]
31. Rehman, A.; Heo, Y.-J.; Nazir, G.; Park, S.-J. Solvent-free, one-pot synthesis of nitrogen-tailored alkali-activated microporous carbons with an efficient CO₂ adsorption. *Carbon* **2021**, *172*, 71–82. [[CrossRef](#)]
32. Rehman, A.; Park, S.-J. From chitosan to urea-modified carbons: Tailoring the ultra-microporosity for enhanced CO₂ adsorption. *Carbon* **2020**, *159*, 625–637. [[CrossRef](#)]
33. Wang, X.; Wang, D.; Song, M.; Xin, C.; Zeng, W. Tetraethylenepentamine-modified activated semicoke for CO₂ capture from flue gas. *Energy Fuels* **2017**, *31*, 3055–3061. [[CrossRef](#)]
34. Quyang, J.; Zheng, C.; Gu, W.; Zhang, Y.; Yang, H.; Suib, S.L. Textural properties determined CO₂ capture of tetraethylenepentamine loaded SiO₂ nanowires from α -sepiolite. *Chem. Eng. J.* **2018**, *337*, 342–350.
35. Zhang, L.X.; Tang, S.Y.; Jiang, C.J.; Jiang, X.Q.; Guan, Y.T. Simultaneous and efficient capture of inorganic nitrogen and heavy metals by polyporous layered double hydroxide and biochar composite for agricultural nonpoint pollution control. *ACS Appl. Mater. Interfaces* **2018**, *10*, 43013–43030. [[CrossRef](#)] [[PubMed](#)]
36. Zhang, L.; Tang, S.; He, F.; Liu, Y.; Mao, W.; Guan, Y. Highly efficient and selective capture of heavy metals by poly(acrylic acid) grafted chitosan and biochar composite for wastewater treatment. *Chem. Eng. J.* **2019**, *378*, 122215–122231. [[CrossRef](#)]
37. Ding, S.; Liu, Y. Adsorption of CO₂ from flue gas by novel seaweed-based KOH-activated porous biochars. *Fuel* **2020**, *260*, 116382–116391. [[CrossRef](#)]
38. Yaumi, A.L.; Abu Bakar, M.Z.; Hameed, B.H. Reusable nitrogen-doped mesoporous carbon adsorbent for carbon dioxide adsorption in fixed-bed. *Energy* **2017**, *138*, 776–784. [[CrossRef](#)]
39. Dong, X.; Ma, L.Q.; Zhu, Y.; Li, Y.; Gu, B. Mechanistic investigation of mercury sorption by Brazilian pepper biochars of different pyrolytic temperatures based on X-ray photoelectron spectroscopy and flow calorimetry. *Environ. Sci. Technol.* **2013**, *47*, 12156–12164. [[CrossRef](#)] [[PubMed](#)]
40. Zhang, X.; Zhang, S.; Yang, H.; Shi, T.; Chen, Y. Influence of NH₃/CO₂ modification on the characteristic of biochar and the CO₂ capture. *Bioenergy Res.* **2013**, *6*, 1147–1153.
41. Xu, Y.; Yang, Z.; Zhang, G.; Zhao, P. Excellent CO₂ adsorption performance of nitrogen-doped waste biocarbon prepared with different activators. *J. Clean. Prod.* **2020**, *264*, 121645–121654. [[CrossRef](#)]
42. Elmouwahidi, A.; Zapata-Benabithé, Z.; Carrasco-Marín, F.; Moreno-Castilla, C. Activated carbons from KOH-activation of argan (*Argania spinosa*) seed shells as supercapacitor electrodes. *Bioresour. Technol.* **2012**, *111*, 185–190. [[CrossRef](#)] [[PubMed](#)]
43. Ello, A.S.; Souza, L.K.C.D.; Trokourey, A.; Jaroniec, M. Development of microporous carbons for CO₂ capture by KOH activation of African palm shells. *J. CO₂ Util.* **2013**, *2*, 35–38. [[CrossRef](#)]
44. Chen, J.; Yang, J.; Hu, G.; Hu, X.; Li, Z.; Shen, S.; Radosz, M.; Fan, M. Enhanced CO₂ capture capacity of nitrogen-doped biomass-derived porous carbons. *ACS Sustain. Chem. Eng.* **2016**, *4*, 1439–1445. [[CrossRef](#)]
45. Vargas, D.P.; Balsamo, M.; Giraldo, L.; Erto, A.; Lancia, A.; Moreno-Piraján, J.C. Equilibrium and dynamic CO₂ adsorption on activated carbon honeycomb monoliths. *Ind. Eng. Chem. Res.* **2016**, *55*, 7898–7905. [[CrossRef](#)]
46. Plaza, M.G.; Pevida, C.; Arias, B.; Feroso, J.; Casal, M.D.; Martín, C.F.; Rubiera, F.; Pis, J.J. Development of low-cost biomass-based adsorbents for post combustion CO₂ capture. *Fuel* **2009**, *88*, 2442–2447. [[CrossRef](#)]
47. Plaza, M.G.; González, A.S.; Pis, J.J.; Rubiera, F.; Pevida, C. Production of microporous biochars by single-step oxidation: Effect of activation conditions on CO₂ capture. *Appl. Energy* **2014**, *114*, 551–562. [[CrossRef](#)]
48. Ma, Z.; Yang, Z.; Zhang, H.; Liu, Z. Nitrogen-doped microporous carbon materials with uniform pore diameters: Design and applications in CO₂ and H₂ adsorption. *Micropor. Mesopor. Mat.* **2020**, *296*, 109992–109998. [[CrossRef](#)]
49. Sarwar, A.; Ali, M.; Khoja, A.H.; Nawar, A.; Waqas, A.; Liaquat, R.; Naqvi, S.R.; Asjid, M. Synthesis and characterization of biomass-derived surface-modified activated carbon for enhanced CO₂ adsorption. *J. CO₂ Util.* **2021**, *46*, 101476–101489. [[CrossRef](#)]
50. Wang, X.; Zeng, W.; Xin, C.; Kong, X.; Hu, X.; Guo, Q. The development of activated carbon from corncob for CO₂ capture. *RSC Adv.* **2022**, *51*, 33069–33078. [[CrossRef](#)]
51. Wang, X.; Zeng, W.; Kong, X.; Xin, C.; Dong, Y.; Hu, X.; Guo, Q. Development of low-cost porous carbons through alkali activation of crop waste for CO₂ capture. *ACS Omega* **2022**, *50*, 46992–47001. [[CrossRef](#)]
52. Pramanik, P.; Patel, H.; Charola, S.; Neogi, S.; Maiti, S. High surface area porous carbon from cotton stalk agro-residue for CO₂ adsorption and study of techno-economic viability of commercial production. *J. CO₂ Util.* **2021**, *45*, 101450–101461. [[CrossRef](#)]
53. Bahamon, D.; Alkhatib, I.I.; Alkhatib, N.; Builes, S.; Sinnokrot, M.; Vega, L.F. A comparative assessment of emerging solvents and adsorbents for mitigating CO₂ emissions from the industrial sector by using molecular modeling tools. *Front. Energy Res.* **2020**, *8*, 165–180. [[CrossRef](#)]

54. Salih, H.A.; Alkhatib, I.I.I.; Zahra, M.A.; Vega, L.F. Diamine based hybrid-slurry system for carbon capture. *J. CO₂ Util.* **2023**, *68*, 102383–102393. [[CrossRef](#)]
55. Singh, G.; Kim, I.Y.; Lakhi, K.S.; Srivastava, P.; Naidu, R.; Vinu, A. Single step synthesis of activated bio-carbons with a high surface area and their excellent CO₂ adsorption capacity. *Carbon* **2017**, *116*, 448–455. [[CrossRef](#)]

Disclaimer/Publisher’s Note: The statements, opinions and data contained in all publications are solely those of the individual author(s) and contributor(s) and not of MDPI and/or the editor(s). MDPI and/or the editor(s) disclaim responsibility for any injury to people or property resulting from any ideas, methods, instructions or products referred to in the content.